Mon. Not. R. Astron. Soc. **000**, 000–000 (0000) Printed 29 August 2011 (MN LaTeX style file v2.2)

arXiv:1108.5242v1 [astro-ph.GA] 26 Aug 2011

Application of three body stability to globular clusters II: observed velocity dispersions

Gareth F. Kennedy[1,2]⋆
[1] *Monash Centre for Astrophysics, Monash University, Clayton, Vic, Australia, 3800*
[2] *School of Chemistry, Monash University, Clayton, Vic, Australia, 3800*

29 August 2011

ABSTRACT

The velocity dispersion profile in globular clusters (GCs) is explained here without having to rely on dark matter or a modification of Newtonian dynamics (MOND). The flattening of the velocity dispersion at large radii in certain Milky Way GCs, or lack thereof, is explained by recourse to the stability of the three-body problem in Newtonian dynamics. The previous paper in this series determined an analytical formula for the transition radius between stable and unstable orbits for a star in a globular cluster. This stability boundary is used here to predict where the velocity dispersion profile is expected to flatten in GCs, given known orbital parameters of the GC-galaxy orbit. Published observational data for the velocity dispersion as a function of radius of 8 Milky Way globular clusters with approximately known orbital parameters has been used here.

We find that the stability radius predicts where the velocity flattens as well as, and in some cases better than, the MOND models do. In particular it is noted that the cluster masses in the MOND models are often incompatible with the velocity dispersion requirements in the inner region of the cluster. However when the stability boundary is determined from the stability in the three-body problem using Newtonian dynamics, it is found to fit the observations well, and there is no need for any MOND type theories to explain the observations. A warning is also made against fitting the velocity dispersion of globular clusters without knowing their orbital parameters, particularly for clusters with strong evidence of ongoing tidal disruption, such as NGC 288.

Key words: gravitation stellar dynamics methods: analytical stars: kinematics globular clusters: general

1 INTRODUCTION

Globular clusters are thought to contain no dark matter, either due to their formation or to the evaporation of low mass dark matter particles (Baumgardt & Mieske 2008). In the case of subsequent evaporation, dark matter may still be present in the outer regions of some clusters. However, for most clusters dark matter can safely be assumed to be absent from the cluster. This means that the cluster density and velocity dispersion profiles should fall off as predicted by a Newtonian dynamics model of a cluster in equilibrium.

The recent discovery of flattening in the velocity dispersion profile for the galactic globular clusters Ω Cen and M15 (Scarpa et al. 2003), where dark matter is thought not to exist, has generated a lot of excitement with some studies claiming that this is direct evidence for a breakdown of Newton's laws at low accelerations. Explanations for the observed deviation broadly fit into three categories; tidal interactions, dark matter or a modified gravity theory (e.g. MOND). All of these theories can produce a flattening of the velocity dispersion profile for large radii, in the case of MOND this occurs at the critical acceleration of 1.2×10^{-10} m/s^2 (Milgrom 1983).

Distant GCs have long been considered as a test of different gravity theories (e.g. Baumgardt et al. 2005; Moffat & Toth 2008), provided that the velocity dispersion profile is sufficiently resolved by being based on 30-80 stars in each cluster (Haghi et al. 2011). At present the statistics are not quite sufficient to rule out MOND, for example in the case of Pal 14 (Gentile et al. 2010).

A distant cluster that has received a lot of recent attention in the literature is NGC 2419. This cluster is located approximately 90 kpc from the galaxy and as such, tidal interactions with the galaxy are expected to be negligible.

⋆ Corresponding author email: gareth.f.kennedy@gmail.com

In addition it is a very luminous cluster and contains many bright giants suitable for spectroscopic analysis, greatly aiding the accuracy of the velocity dispersion profile.

The velocity dispersion profile of NGC 2419 can only be fit using the MOND acceleration cut-off if there is substantial radial anisotropy in the cluster (Sollima & Nipoti 2010). The effect of radial anisotropy was found to be stronger in a MOND cluster profile than their equivalent Newtonian systems (Nipoti et al. 2011). While there is some radial anisotropy due to rotation, Baumgardt et al. (2009) found that there is not enough to reconcile the velocity dispersion with MOND. NGC 2419 is most likely to be a remnant of a much larger system as evidenced dynamically (Baumgardt et al. 2009) and chemically (Di Criscienzo et al. 2011), which complicates the picture but still fails to reconcile the observations to any MOND model. A more recent and comprehensive comparison between Newtonian and MOND models to an increased data set for NGC 2419 by Ibata et al. (2011) found that the best MOND fit was far worse than the best Newtonian Michie model by a factor of 40000.

For closer GCs, recent observational studies have found that MOND or dark matter is not required in many GCs. For example Lane et al. (2010) (and references therein) found that of the 10 GCs studied, the velocity dispersion profiles of all except NGC 6121 (M4) could be well fit using a Plummer sphere model. They found that M4 had a mass of twice the literature values due to tidal heating increasing the velocity dispersion in the outer regions. The velocity distribution of this cluster was also complicated by the clear signature of cluster rotation found in the observations.

The premise of this paper is that the velocity dispersion profile is expected to flatten out in the region where orbits become unstable. The method used for determining the stability boundary is summarised here based on the previous paper in this series (Kennedy 2011, hereafter Paper I) which was based on the stability of the general three-body problem as derived in Mardling (2008b) and Mardling (2008a). This will occur in the Newtonian dynamics regime without need for any modifications to the theory of gravity or additional dark matter. The determination of this radius for a Plummer sphere is summarised in Section 2 and is given in more detail in Paper I. This section also covers the velocity dispersion as a function of radius for Newtonian dynamics and the radius where this profile is predicted to break down according to MOND. A simulated cluster model is used in Section 3 to show that the velocity dispersion profile does indeed flatten where stars exist in unstable orbits.

The bulk of the paper is devoted to comparing the predicted radius of flattening velocity dispersion to 8 individual cluster observations from the Milky Way globular cluster system (Section 5). These GCs are selected on the basis that data is available on the velocity dispersion as a function of radius and on the velocity of the cluster, which is used to determine the parameters for the cluster-galaxy orbit. This section includes a discussion on any discrepancies between our predictions using the stability boundary and those by MOND for particular globular clusters. Conclusions are drawn in Section 6, in particular that modified gravity theories are not needed to explain the observations.

2 STABILITY BOUNDARY IN A PLUMMER SPHERE

The previous paper in this series outlined a simple method for determining the transition between stable interior and unstable exterior orbits in a GC. An unstable system is taken to mean that a star is on an orbit that makes the total system unstable to the escape of one of the bodies. In the context of GCs this is equivalent to the eventual escape of a star from the potential well of the cluster. Kennedy (2011) used this stability boundary to estimate the tidal radius for a cluster given its galactic orbital parameters of perigalacticon (R_p) and eccentricity (e). This radius was derived assuming point masses for the distant galaxy and stars orbiting within the cluster, which is described by a Plummer potential centred on the cluster core. In this section we give an overview of the results from this paper where they are relevant to predicting the flattening of the velocity dispersion in GCs.

A globular cluster is modelled using a Plummer sphere with gravitational potential given by (Binney & Tremaine 1987)

$$\Phi = \frac{-GM_C}{\sqrt{r_{1/2}^2 + r^2}} \tag{1}$$

where G is the gravitational constant, M_C is the mass of the cluster, r is the radial distance, and $r_{1/2}$ is the observable half mass radius of the cluster for a projected velocity dispersion.

Dejonghe (1987) gives the velocity dispersion as a function of cluster radius, r, for a Plummer sphere to be

$$\sigma^2(R) = \frac{\sigma_0^2}{\sqrt{1 + \frac{r^2}{r_{1/2}^2}}} \tag{2}$$

and the central velocity dispersion (σ_0) is related to the cluster mass M_C by

$$M_C = \frac{64\sigma_0^2 r_{1/2}}{3\pi G} \tag{3}$$

where G has its usual value.

Throughout this paper there are two radii of key importance for each GC. These are the radius where the acceleration acting on a star due to the cluster potential goes beneath the MOND limit of $a_0 = 1.2 \times 10^{-10}$ m/s^2 (r_{a0}), and the radius of the transition between stable and unstable orbits (r_{chaos}, see below). Firstly the MOND radius is found by iterating over the acceleration a_0 and solving for r_{a0}, which for a Plummer sphere is

$$a_0 = \frac{GM_C r_{a0}}{\left(r_{1/2}^2 + r_{a0}^2\right)^{3/2}} \tag{4}$$

given the known values of $r_{1/2}$ and M_C.

For the second radius we adopt a functional form for the tidal radius that is separable into a mass component and orbital eccentricity of the cluster-galaxy orbit

$$r_t = R_p \left(\frac{M_C}{M_G}\right)^{1/3} f(e) \tag{5}$$

where M_C and M_G are the masses of the cluster and galaxy respectively, e is the eccentricity of the cluster orbit around the galaxy, and R_p is the distance of closest approach to the

Table 1. Coefficients for the polynomial fit to r_{chaos} and the minimum and maximum extents of the marginally chaotic zone.

	r_{chaos}	r_{min}	r_{max}
a_0	-0.897753	-0.892899	-0.888868
a_1	-2.28272	-1.83631	-1.93401
a_2	16.8616	10.3382	13.844
a_3	-74.0133	-45.1384	-63.0546
a_4	177.136	108.206	163.39
a_5	-236.158	-144.186	-239.155
a_6	163.999	99.5267	182.311
a_7	-46.3734	-27.6654	-56.3393

For radii $r < r_{min}$ all orbits are expected to be stable, whereas for $r > r_{max}$ they are expected to be chaotic. The resultant functions of the eccentricity of the cluster-galaxy orbit are shown in Figure 1. For details on how these coefficients are determined see Kennedy (2011).

galaxy, referred to as perigalacticon. This form of the tidal radius also allows direct comparison between the stability boundary and other tidal radii estimates from the literature.

The most commonly used tidal radius estimate is for a star on a radial orbit and using point mass potentials for the cluster and galaxy. The eccentricity dependence, $f(e)$, of the tidal radius is given by the classical King (1962) result

$$f(e) = k\,(3+e)^{-1/3} \tag{6}$$

where the constant $k \sim 0.7$ was introduced by Keenan (1981) to better fit observations of the galactic globular clusters. The King radius (r_t) will be used to denote the maximum theoretical tidal radius of a GC by using Equations (5) and (6) with $k = 1$ and $e = 0$.

The stability boundary was determined in Paper I using the eccentricity distribution for stars in an isolated cluster as modelled by a Plummer sphere of potential given by Equation 1. The transition between stable interior orbits and unstable exterior orbits was not a single value; rather it was a range of radii that depended on the eccentricity of the cluster-galaxy orbit. To describe this transition three values were used, the minimum and maximum values and an indicative value denoted by r_{chaos}. This value was defined as the lowest radius where the fraction of unstable orbits drops beneath 10%.

Using the same form for the tidal radius as Equation (5) with the same mass dependence then the eccentricity dependence for all three values can be fit using a Taylor series in e of the form

$$f(e) = \exp\left[\sum_{i=0}^{N=7} a_i e^i\right] \tag{7}$$

where the coefficients are given in Table 1 for the indicative stability boundary radius (r_{chaos}) and the minimum and maximum extents of the partially stable region. For radii $r < r_{min}$ all orbits are expected to be stable, whereas for $r > r_{max}$ they are expected to be chaotic. The eccentricity dependence for $r_{min/max}$ and r_{chaos} as a function of the eccentricity of the cluster-galaxy orbit are shown in Figure 1.

The functional dependence on the eccentricity was derived using a distribution of stellar orbital eccentricities and was effectively independent of the cluster mass. The assumption of a point mass potential for the galaxy for distant cluster orbits is justified for distant GCs since the mass inside 6.4 kpc is consistent with that of a point mass of roughly $10^{11} M_{\odot}$, based on the orbits of NGC 2419 and NGC 7006 (Bellazzini 2004). However all of the GC orbits examined here have perigalacticon distances (R_p) inside 6 kpc. The procedure adopted in Section 4 determines an effective Keplerian orbit by setting $R_p = R_p(min)$ and getting the eccentricity from the apogalacticon $R_a = R_amax$ from multiple passages. This means that the orbital parameters are themselves an approximation of a Keplerian orbit to a more complicated orbit. In this context the error in the GC-galaxy orbit due to modelling the galaxy as a point mass is negligible. The overall effect of the uncertainties in the GC-galaxy orbit is discussed in Section 5.

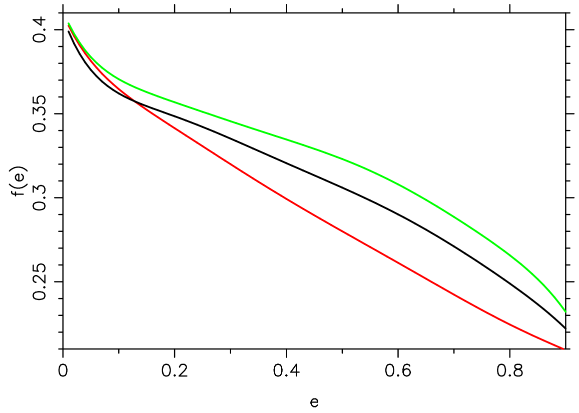

Figure 1. The eccentricity dependence for the transition from stable inner orbits to unstable exterior orbits. The form of the eccentricity dependence is given by Equation 7 with coefficients given in Table 1 and the corresponding radius is given by Equation 5. The indicative value for the stability boundary (associated with r_{chaos}) is shown as black, while the minimum and maximum extents of the partially stable region are the red and green curves respectively.

As pointed out by Fukushige & Heggie (2000) the tidal radius does not act as an instant remover of stars. They found for GCs on circular orbits that the escape timescales for stars beyond the tidal radii could be long enough to allow some stars to stay in this region indefinitely. This means that the predicted tidal radius will be a lower limit as stars outside this can still be close to the GC while remaining formally unbound. Stars on such unstable orbits will be observable inside the King radius, but are expected to have very different velocities compared to an equilibrium cluster. The effect of stars on these orbits on the observable velocity dispersion profile is discussed in the next section.

3 VELOCITY DISPERSION PROFILE IN A SIMULATED CLUSTER

It is expected that stars on chaotic orbits at large distances from the cluster centre lead to a different velocity profile than an equilibrium model (such as Equation 2). This section uses a simple cluster model to estimate what effect stars on chaotic orbits in the outer regions of a globular cluster has on the velocity dispersion profile.

A globular cluster is modelled using a Plummer sphere with gravitational potential given by Equation (1) centred on a single particle that in turn orbits the galaxy. To examine the effect of the tidal field, without prescribing the force as a function of time, a free moving point mass particle of mass $10^{11} M_\odot$ is used. The stars in the outer regions of the cluster are modelled as point masses of $1 M_\odot$ that respond to the movement of the cluster centre particle of $10^6 M_\odot$, but not to each other. This same model was used in Paper I, without the inclusion of the galactic tidal field, to determine the distribution of orbital eccentricities for stars inside the cluster in finding the stability boundary.

By removing the mutual interactions between particles the cluster model does not include two-body relaxation. This is not a problem for the outer regions of interest here since typical relaxation timescales are greater than 1 Gyr at the half mass radius and scale as approximately $r^{1/2}$. Therefore the relaxation timescale in the outer cluster regions is close to the age of the cluster itself and the region is collisionless. There is a form of relaxation due to the cluster centre particle moving in response to the distribution of cluster halo stars. The wandering of the cluster centre moves the Plummer potential which accelerates the loss of stars over the tidal radius. From extensive simulations it was found that the wandering core is not a problem until the cluster has lost most of its original mass. At this point the cluster is strongly disrupted and its velocity dispersion cannot be adequately described by a simple equilibrium model.

The primary interest here is to observe deviations from the velocity dispersion for a cluster in equilibrium, given by Equation (2), thus the distribution of stars is artificially biased to provide better resolution in the outer regions. A uniform distribution in radius between $r_{1/2}$ and the King radius r_t is chosen and sampled with 10^3 stars. The region inside $r_{1/2}$ is modelled by an unchanging potential rather than particles since the velocity distribution inside the half mass radius remains isotropic and therefore does not need to be resolved (e.g. Giersz & Heggie 1994). All particles are numerically integrated for a total of 30 cluster-galaxy orbits ($\approx$ 4.4 Gyr) using a collisionless N-body code with a Bulirsch-Stoer integrator (Press et al. 1986) that conserves energy and angular momentum. Further details about the model are described in Kennedy (2008).

Many models were run to sample across a range of cluster-galaxy orbital parameters; here we focus on one model where the stability boundary was well resolved. The system parameters are $R_p = 1000 r_{1/2}$, $e_{out} = 0.3$ and $r_{1/2} = 1$pc, $M_C = 10^6 M_\odot$ and $M_G = 10^{11} M_\odot$. The velocity dispersion profile against radial distance to the cluster centre after 10 (black), 20 (red) and 30 (green) cluster-galaxy orbital periods are shown in Figure 2. All time snapshots are taken at the apogalacticon to reduce any spurious perturbations to the halo stars from perigalacticon passages. The transition between stable and unstable orbits (r_{chaos}) is shown as a solid vertical line, with the range ($r_{min/max}$) shaded to show the size of the transition. The radius for which the acceleration is equal to the MOND value, given by Equation 4, is shown as a dashed vertical line.

As is evident from Figure 2, the stability boundary is a good predictor for the flattening of the velocity dispersion. Coincidently the MOND radius for this cluster also occurs before the flattening despite the purely Newtonian dynamics included in the simulation. The occurrence of flattening in the velocity dispersion and its accurate prediction by the stability boundary provides confidence applying this method to observations of GCs in the Milky Way system in Section 5.

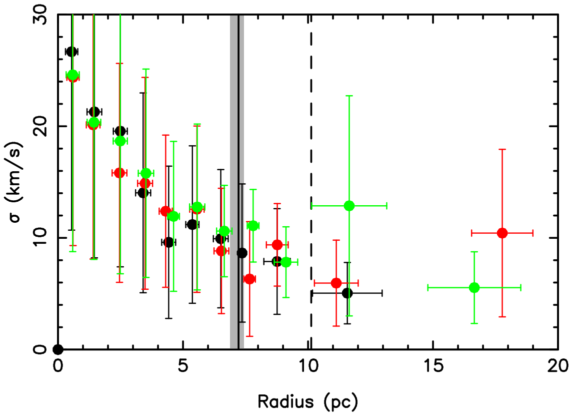

Figure 2. The velocity dispersion profile against radius from a collisionless N-body cluster simulation composed of 1000 particles. The velocity dispersion profile after 10 (black), 20 (red) and 30 (green) cluster-galaxy orbits is shown. The transition from stable inner to unstable outer orbits is shaded and the indicative radius (r_{chaos}) is shown as a vertical line. The radius for which the acceleration is equal to the MOND value is shown as a dashed vertical line. Note that the velocity dispersion begins to flatten in the outer unstable region.

4 DETERMINATION OF GC-GALAXY ORBITS

Before comparing the velocity dispersion profiles of real clusters to the radii estimates in Section 2 the orbital parameters of the cluster-galaxy orbit are required. In this section the galactic orbits of 8 GCs are determined based on the observed velocities for each cluster and integrating backwards in time through a realistic galactic potential. The perigalacticon (R_p) and eccentricity (e) can then be obtained from the integrated orbits for each GC.

Recent velocity and distance values for each cluster (references in Table 2) are used in conjunction with the galactic potential used by Fellhauer et al. (2007). This gravitational potential consists of a Miyamoto-Nagai potential (Miyamoto & Nagai 1975) combined with a logarithmic potential. The total galactic potential Φ is given as a sum of the galactic halo Φ_h, disc Φ_d and bulge Φ_b potentials by (Fellhauer et al. 2007)

$$\Phi(x, y, z) = \Phi_h(r) + \Phi_d(R, z) + \Phi_b(r) \tag{8}$$

where

$$r = \sqrt{x^2 + y^2 + z^2} \qquad R = \sqrt{x^2 + y^2} \tag{9}$$

and x, y and z are galactic coordinates with units in kpc. In this coordinate system the Sun is located at (-8,0,0) at which a particle with velocity directed in the positive **y** direction is moving in the direction of Galactic rotation. It follows that **z** points in the direction of the northern galactic pole. The gravitational potentials for the galactic halo Φ_h, disc Φ_d and bulge Φ_b are

$$\Phi_h(r) \quad = \quad \frac{1}{2} v_o^2 \ln\left(1 + \frac{r^2}{a^2}\right) \tag{10}$$

$$\Phi_d(R,z) = \frac{-GM_d}{\sqrt{R^2+\left(b+\sqrt{z^2+c^2}\right)^2}} \quad (11)$$

$$\Phi_b(r) = \frac{-GM_b}{r+d} \quad (12)$$

where $a = 12.0$ kpc, $b = 6.5$ kpc, $c = 0.26$ kpc, $d = 0.7$ kpc, $v_o = 181$ km/s and G is the gravitational constant. The masses of the galactic disc and bulge are $M_d = 10^{11}$ $M_\odot$ and $M_b = 3.5 \times 10^{10}$ $M_\odot$ respectively. The equations of motion for a cluster moving in this potential are given by

$$\ddot{\mathbf{r}} = -\nabla\left(\Phi_h + \Phi_d + \Phi_b\right). \quad (13)$$

For globular clusters with velocity data given in the literature, Equation (13) is integrated back through time for approximately 10 cluster-galaxy orbits, using the Bulirsch-Stoer numerical integration method (Press et al. 1986). Then r_{min} and r_{max} are measured and used to approximate the effective Keplerian orbital eccentricity and perigalacticon.

The initial conditions and resulting orbital parameters from these cluster-galaxy orbit simulations are summarised in Table 2. This table lists the observed cluster mass (M_C), the distance to the galactic centre (R_G), orbital parameters (R_p, e), half-mass radius ($r_{1/2}$), the region where the velocity dispersion flattens (r_{flat}), the theoretical estimates where this will occur (r_{chaos} and r_{a0}), the tidal radius given by Equation (5) and finally the references for orbital and velocity dispersion observational data. The orbital parameters R_p, e and P for the GCs in Table 2 generally agree with the parameters found by Allen et al. (2006) who used a different galactic potential.

Note that there are two sets of masses (M_C) for each cluster in Table 2. The first of these sets contains the MOND paper cluster masses quoted in Scarpa et al. (2011) (and references therein) and fitted such that r_{a0} is close to r_{flat}. The second mass set is determined using the central velocity dispersion for each cluster from a fit to all data points within r_{a0}, where the cluster is in the Newtonian regime and Equations (2) and (3) are valid.

Most of the uncertainty in the orbital parameters (R_p and e) is due to the observations of the cluster velocity components directed tangential to our line of sight having large uncertainties. Such measurements are difficult to obtain and rely on comparing the current positions of globular clusters on the sky with older position data found on photographic plates. The motion of each cluster is then determined from the change in positions (in milli-arcseconds) over time, with the positions calibrated using "fixed" distant objects, such as quasars (e.g. Dinescu et al. 1997). The error is also amplified by uncertainties in the distance to the cluster, which also affects the half-mass radius measurement. From the point of view of the orbital parameters in Table 2 these uncertainties are most likely to translate to an error in eccentricity if $R_p/R_G \sim 1$ and in eccentricity and perigalacticon if $Rp << Rg$. It is proposed here that the error in the cluster-galaxy orbital parameters is the reason for discrepancies in the velocity dispersion profile for particular clusters in the next section.

5 GC VELOCITY DISPERSION PROFILES

This study is limited to clusters for which online data is available for the velocity dispersion as a function of radius where flattening has been reported. We are further limited to clusters where the orbital parameters can be determined (previous section). The galactic globular clusters fitting these requirements are listed in Table 2.

Observational data for the velocity dispersion profiles for each cluster are given in Table 2 along with the data sources for each cluster. Most velocity dispersion data available online was from Scarpa et al. (2011) (and references therein) who chose cluster masses consistent with the MOND radius fitting the flattened region. These masses are collectively referred to as the MOND cluster masses and are listed first in Table 2 for each cluster. Distances to the galactic centre (R_G) for all clusters were taken from Harris (1996). References for the orbital parameters are listed in the table as numbers rather than letters for each cluster.

Two special cases for the observed velocity dispersion data exist in this sample. Firstly, the velocity dispersion data for NGC 7078 are taken from the non-rotating cluster model favoured by Drukier et al. (1998), rather than the rotating cluster model. Secondly, the velocity dispersion data for NGC 6341 (Drukier et al. 2007) was not binned in radius in the same way as the other clusters in this sample. For this cluster no data was given on the minimum or maximum distances for each bin, nor for the number of stars used in each bin. This means that no radial error bars are available for the data points for NGC 6341.

Figures 3 and 4 show the velocity dispersion profiles for all clusters listed in Table 2 using the MOND cluster masses. The MOND radius r_{a0} as calculated for each cluster from Equation (3) is shown in each plot as a dashed red line. For the MOND masses this is close to where the velocity dispersion flattens out by the choice of the cluster mass M_C. The transition from stable to unstable orbits is shaded in grey and the indicative radius r_{chaos} is shown as a solid line inside this region. The theoretical maximum extent of the cluster, the tidal radius using Equation (6), is shown as a dotted vertical line when it is inside the plotted range. Finally the red dotted curve indicates the theoretical velocity dispersion for the quoted cluster mass using the radial dependence given by Equations (2) and (3).

The second set of masses in Table 2 uses cluster mass values determined by fitting the observational data points within r_{a0}. The fits are calculated by Equations (2) and (3) and the error is minimised using a χ^2 test for all data with $r < r_{a0}$. However since r_{a0} depends on M_C which in turn depends on the data points used to get the fit from which σ_0 is taken then M_C must be solved in an iterative manner. The resulting masses are listed in the table and are also shown next to the names of each cluster in Figures 5 and 6. These figures present the same data as previously shown in Figures 3 and 4, differing only in the cluster mass used to determine the stability transition region, r_{chaos}, r_t, r_{a0} and the theoretical velocity dispersion profile.

The results from Figure 3-6 can be summarised in terms of how close the MOND acceleration radius (r_{a0}) or the transition to unstable orbits (r_{chaos}) fits the flattening of the velocity dispersion. Differences between the MOND and chaotic orbit predictions can be described in three general

Table 2. Globular cluster parameters for 8 Milky Way globular clusters.

Cluster	M_C ($M_\odot$)	R_G (kpc)	R_p (kpc)	e	$r_{1/2}$ (pc)	r_{flat} (pc)	r_{chaos} (pc)	r_{a0} (pc)	r_t (pc)	Refs
NGC 288	4.4×10^4	12.0	1.7	0.74	5.76	0	3.40	0.0	5.8	E,1,2
	6.4×10^4						3.85	0.0	6.6	
NGC 1851	1.8×10^5	16.6	5.7	0.69	1.83	12.5 ± 2.5	18.9	14.5	31.4	H,2
	3.6×10^5						23.9	20.3	39.6	
NGC 1904	1.2×10^5	18.8	4.2	0.65	3.0	12 ± 2	12.5	11.7	20.3	H,2
	1.3×10^5						12.9	11.7	20.8	
NGC 5139	1.1×10^6	6.4	1.2	0.67	7.7	32 ± 3	7.4	35.7	12.1	B,G,1,2
(ω Cen)	2.5×10^6						9.7	52.9	15.9	
NGC 6171	5.9×10^4	3.3	2.3	0.21	3.25	8 ± 2	6.7	8.0	9.2	C,1,2
	8.6×10^4						7.6	9.1	10.4	
NGC 6341	1.6×10^5	9.6	1.4	0.76	2.24	12 ± 2	4.2	13.6	7.4	D,1,2
	1.4×10^5						4.0	12.4	7.1	
NGC 7078	3.9×10^5	10.4	5.4	0.32	3.01	20 ± 2	28.2	21.3	39.9	A,1,2
	3.7×10^5						27.8	20.4	39.2	
NGC 7099	7.8×10^4	7.1	3.0	0.39	2.39	10 ± 2	8.9	9.6	12.9	F,2
	7.6×10^4						8.8	8.9	12.8	

Cluster masses from fits using MOND and from the inner velocity dispersion are given in column 2. Orbital and structural parameters for each cluster are given in columns 3-6. The estimate for the observed flattening is given in column 7 and predictions for this value using the stability boundary and the MOND radius where $a_0 = 1.2 \times 10^{-8}$ cm s^{-2} assuming $M/L = 1$ (Scarpa et al. 2011, and references therein) are given in columns 8 and 9 respectively. The tidal radii as calculated by Equation (5) is given in column 10. The final column contains the references for the orbital parameters (often the raw cluster velocities) and the velocity dispersion profiles. The references are denoted by numbers in the former case and letters in the later and are; A = Drukier et al. (1998), B = Scarpa et al. (2003), C = Scarpa et al. (2004), D = Drukier et al. (2007), E = Scarpa et al. (2007a), F = Scarpa et al. (2007b), G = Scarpa & Falomo (2010), H = Scarpa et al. (2011), 1 = Meziane & Colin (1996) and references therein, 2 = Dinescu et al. (1999) and references therein, 3 = Dinescu et al. (2001). See in-text for more details including how the orbital parameters R_p and e are determined.

categories; estimates are consistent in cluster masses, inconsistent masses, and problem clusters for both models.

5.1 Consistent masses

This category is defined as the set of clusters where the MOND mass and the fitted mass are in good agreement and where both r_{a0} and r_{chaos} are consistent with the flattening of the velocity dispersion. This category includes; NGC 288, NGC 1904, NGC 7078 and NGC 7099.

The velocity dispersion of **NGC 288** is consistent with being completely flat with an average value of 2.3 ± 0.15 km/s (Scarpa et al. 2007a). This cluster has a low concentration cluster with a mass of $\sim 5 \times 10^4 M_\odot$ and a half-mass radius of $r_{1/2} = 5.76$ pc. As such the acceleration due to the cluster potential is below the MOND limit for all values of radius, i.e. $r_{a0} = 0$ pc. The stability boundary and the tidal radius are also very close to the centre of the cluster, as seen in panel (a) of Figures 3 and 5. NGC 288 has a galactic orbit with a low perigalacticon (1.7 kpc) and high eccentricity (0.74) which means that its tidal radius is inside the observable cluster limits; hence it is currently being disrupted. Additional velocity dispersion observational data to 26 pc obtained by Lane et al. (2010) found that a Plummer model provided a good fit to a low concentration cluster without significant deviation from Newtonian dynamics.

In the case of **NGC 7078** r_{a0} is closer to the cluster centre than r_{chaos}, but both radii are consistent with the flattening of the velocity dispersion. The observational data presented in the figures is based on the no rotation model favoured by Drukier et al. (1998). They also put forward the explanation of the flattening in the velocity dispersion as being due to tidal heating, as expected in the models of Allen & Richstone (1988).

For the remaining clusters with consistent masses, **NGC 1904** and **NGC 7099**, we find that $r_{a0} \approx r_{chaos}$. In other words either MOND or the occurrence of chaotic orbits in the outer regions can be used to explain the flattening of the velocity dispersion. This is the general conclusion for all four clusters in this category.

5.2 Inconsistent masses

This category is defined as those where the MOND mass and the fitted mass are in substantial disagreement. In general the r_{a0} is a good fit to the velocity dispersion flattening only when the MOND masses are used, however these are inconsistent with the velocity dispersion profiles in the inner regions where it should by purely Newtonian. This category includes NGC 1851 and NGC 6171.

MOND has particular difficulty fitting the flattening of **NGC 1851** with the fitted cluster mass value of $3.6 \times 10^5 M_\odot$, however the same is true for the stability transition for this cluster. For the MOND cluster mass of $1.8 \times 10^5 M_\odot$ both r_{a0} and r_{chaos} are consistent with the flattening of the velocity dispersion at about 18 pc. It is proposed that there is most likely an error in the orbit ($R_p = 5.7$kpc and $e = 0.69$) for this cluster. For example changing the perigalacticon of the orbit to $R_p = 5$ kpc or increasing the eccentricity both decrease r_{chaos}. However changing the orbit will not change the radius where the acceleration drops beneath the critical MOND value.

The MOND cluster mass given by Scarpa et al. (2004) for **NGC 6171** seems peculiarly lower than the fitted mass,

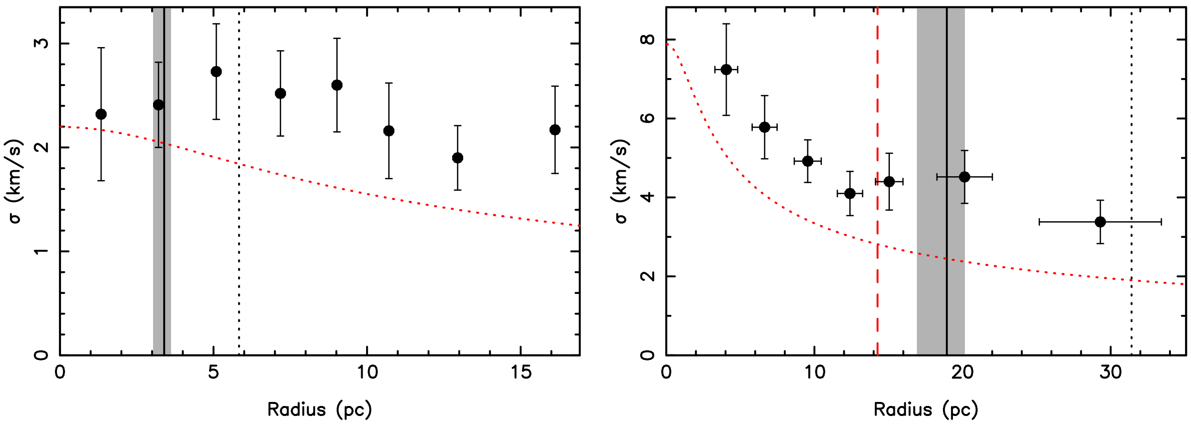
(a) **NGC 288**; $M_C = 4.4 \times 10^4 M_\odot$

(b) **NGC 1851**; $M_C = 1.8 \times 10^5 M_\odot$

[!hp]

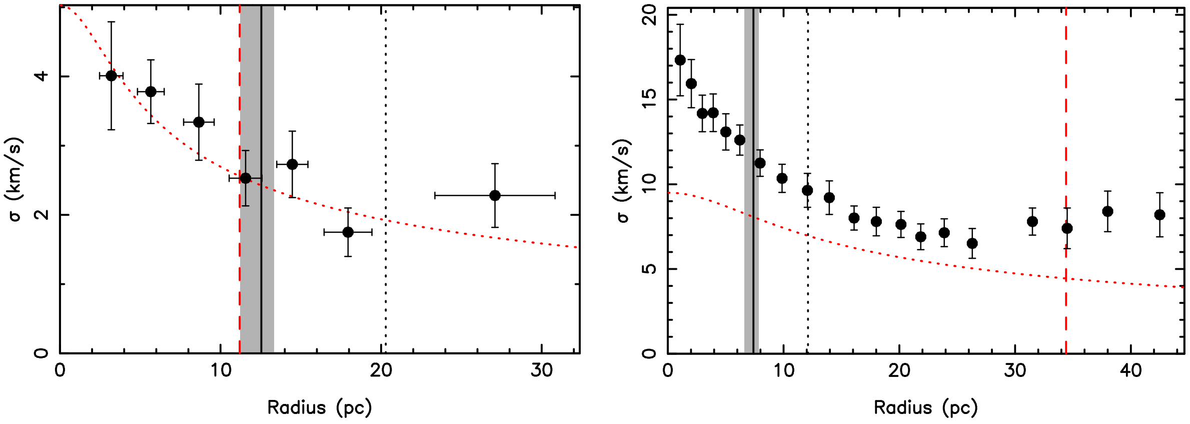
(c) **NGC 1904**; $M_C = 1.2 \times 10^5 M_\odot$

(d) **NGC 5139 (ω Cen)**; $M_C = 1.1 \times 10^6 M_\odot$

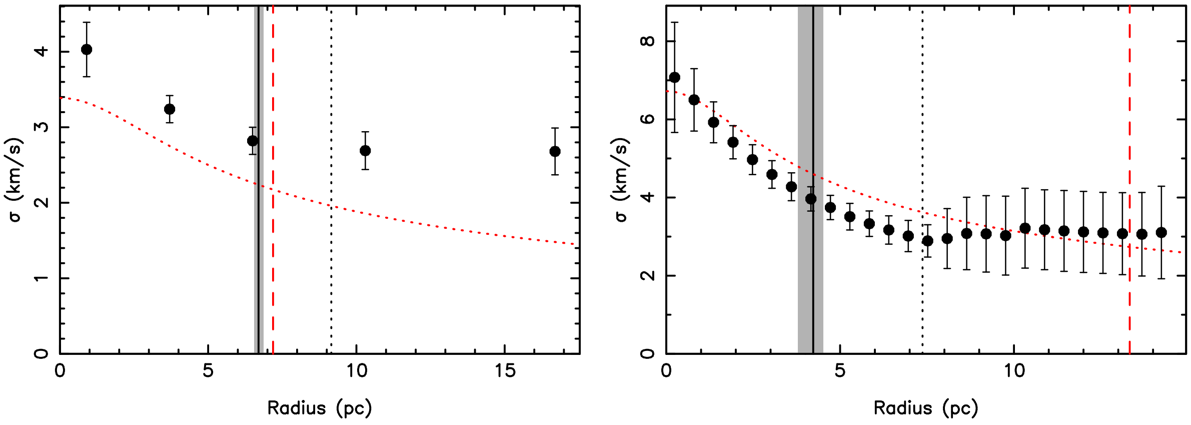
(e) **NGC 6171**; $M_C = 5.9 \times 10^4 M_\odot$

(f) **NGC 6341**; $M_C = 1.6 \times 10^5 M_\odot$

Figure 3. The velocity dispersion profile for all globular clusters in this study using the cluster mass estimates given in MOND papers. Masses are shown beside the cluster name and the other cluster parameters are given in Table 2. The transition from stable to unstable orbits is shaded in grey and the indicative radius r_{chaos} is shown as the solid vertical lines. The vertical red dashed line shows where the acceleration is equal to the MOND value. The red dotted curve indicates the theoretical velocity dispersion for the quoted cluster mass.

particularly since the MOND radius gives a good fit to the flattening of the velocity dispersion in both cases. Interestingly for both masses the stability transition is interior to the MOND radius and as such provides a better fit to the flattening.

The flattening of the velocity dispersion for both of these clusters is found to be a better fit by the stability transition to chaotic orbits than by the radius where the acceleration equals the MOND value.

5.3 Problematic clusters

This category includes the clusters which present consistency problems for both the MOND model and the chaotic

[!hp]

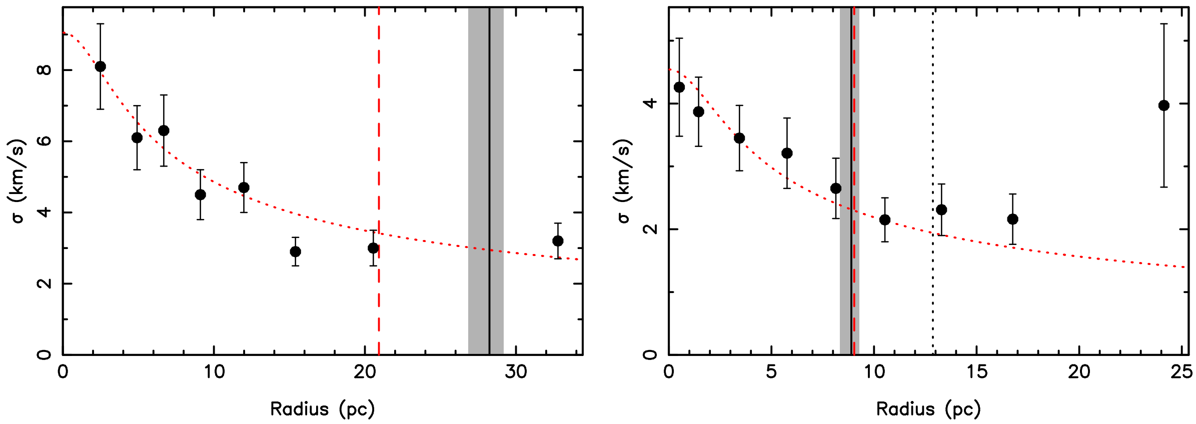

(a) **NGC 7078**; $M_C = 3.9 \times 10^5 M_\odot$

(b) **NGC 7099**; $M_C = 7.8 \times 10^4 M_\odot$

Figure 4. Figure 3 continued; MOND cluster masses used.

orbits model. The two clusters in this category are NGC 5139 (ω Cen) and NGC 6341 and a longer discussion of the results for these clusters is warranted.

As is typical for this cluster, the velocity dispersion profile of **NGC 5139** (ω Cen) presents difficulties for both models. In the case of MOND the radius r_{a0} can be made to roughly match the observed flattening near 30 pc only by using a mass of $M_C = 1.1 \times 10^6 M_\odot$. However this mass is not compatible with the velocity dispersion inside the cluster in the Newtonian regime, which requires a mass of $M_C = 2.5 \times 10^6 M_\odot$. Using chaotic orbits for this cluster is also difficult in that the stability boundary is found to be well inside the cluster for the orbital parameters given in Table 2. Two possible resolutions to this incompatibility might come from the fact that NGC 5139 is likely to be rapidly rotating (e.g. Scarpa & Falomo 2010) and/or that it is suffering ongoing disruption (see below).

The final cluster examined in this study is **NGC 6341** which has a cluster mass of approximately $M_C = 1.5 \times 10^5 M_\odot$ by both the MOND literature and the fitting procedure used here. The MOND radius of $r_{a0} = 13$ pc is significantly exterior to the observed velocity dispersion, flattening at about 8 pc, which is itself exterior to the predicted stability boundary of $r_{chaos} = 4$ pc. A key observation for this cluster is that the flattening occurs very close to the tidal radius itself. This implies that the cluster is being severely tidally disrupted which explains the flattening without need for MOND.

Both of these clusters, especially NGC 6341, have evidence of ongoing tidal disruption. Note that neither the tidal radius nor the stability boundary act as an instant remover of stars, as pointed out by Fukushige & Heggie (2000). They found for GCs on circular orbits that the escape timescales for stars beyond the tidal radii could be long enough to allow some stars to stay in this region indefinitely. For eccentric cluster-galaxy orbit this timescale would be shorter while for internal orbits within the cluster the timescale would be substantially longer. It seems likely that this effect is seen in both NGC 5139 and NGC 6341.

An alternative explanation for these clusters is that the orbital parameters are in error. As mentioned previously the eccentricity (e) and to a lesser extent the perigalacticon (R_p) have large uncertainties. Changing either of these quantities has a dramatic effect on the estimate for r_{chaos} but no effect on the position of r_{a0} when only the cluster potential is considered. For example an increase in eccentricity of $\Delta e \sim 0.1$ will produce approximately a 10% decrease in r_{chaos}, for a fixed value of R_p. While this may be sufficient to explain NGC 6341, it is not sufficient to explain NGC 5139 which may require a higher initial mass and ongoing tidal disruption to explain the velocity dispersion.

6 CONCLUSIONS

It is found that MOND is not required to explain the flattening of the velocity dispersion profile in globular clusters. We examined eight GCs from the Milky Way GC system with observational data for both the velocity dispersions as a function of radius from the cluster centre and with data for the orbital parameters for the cluster-galaxy orbit.

From all of these clusters we found that the flattening could be equally, if not better, predicted using the transition from stable interior to unstable exterior orbits than using the radius where the acceleration equals the MOND value. Of the eight clusters, a minor change in the perigalacticon and eccentricity of NGC 1851, and more substantial changes to those for NGC 6341, would result in a much better fit using the stability results in the Newtonian regime than the MOND predictions. Since the orbital parameters are determined from observations of the proper motions of the clusters, these quantities are known to be very uncertain. In the case of NGC 6341 the errors in the orbital parameters need not be so large if the cluster is undergoing substantial tidal disruption, as seems likely.

One missing feature in the analysis of the velocity dispersion profiles of GCs presented here is the non-rigorous treatment of cluster rotation. For example Székely et al. (2007) studied five clusters (NGC 104, NGC 288, NGC 6218, NGC 7099 and NGC 6809) and found evidence for rotation in four of them. They also emphasise the point that to disentangle these effects from a possible breakdown of Newtonian dynamics would require observations of a much larger range of globular clusters. We would add to this that the orbital parameters must be known in order to do any meaningful

(a) **NGC 288**; $M_C = 6.4 \times 10^4 M_\odot$ (b) **NGC 1851**; $M_C = 3.6 \times 10^5 M_\odot$

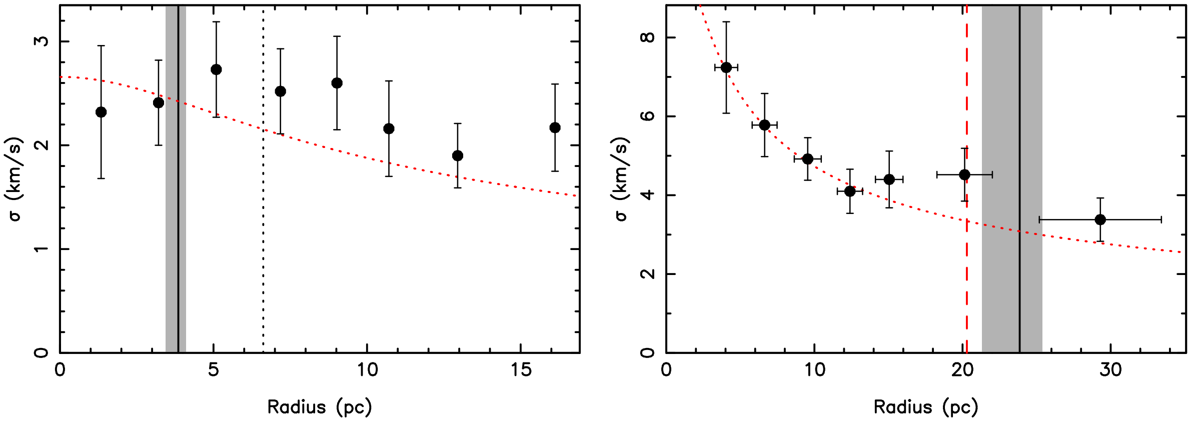

(c) **NGC 1904**; $M_C = 1.3 \times 10^5 M_\odot$ (d) **NGC 5139 (ω Cen)**; $M_C = 2.5 \times 10^6 M_\odot$

[!hp]

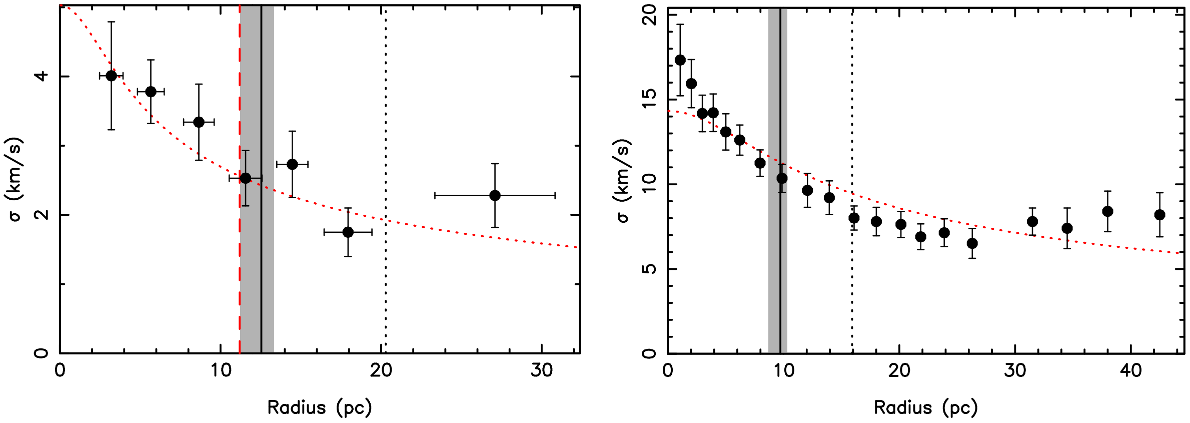

(e) **NGC 6171**; $M_C = 8.6 \times 10^4 M_\odot$ (f) **NGC 6341**; $M_C = 1.4 \times 10^5 M_\odot$

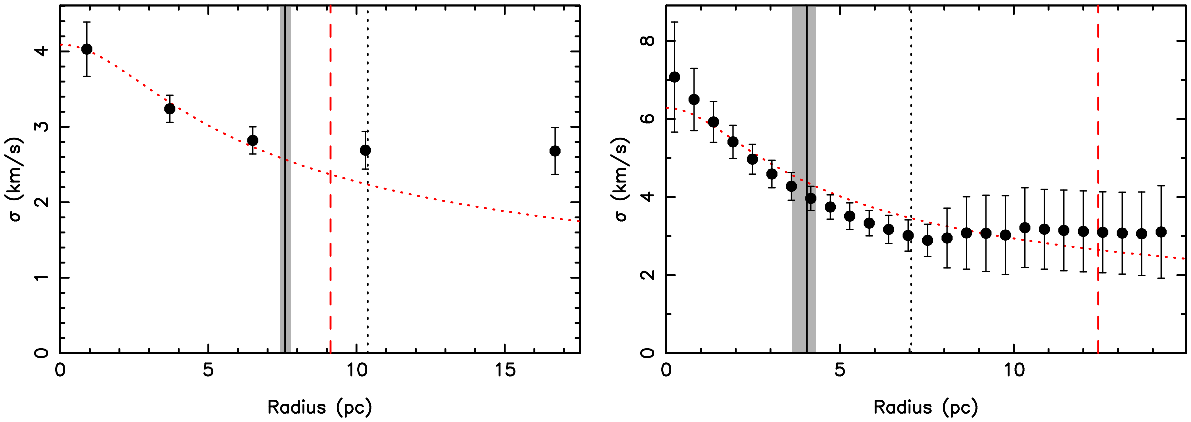

Figure 5. Velocity dispersion for all globular clusters in this study using mass estimates from the fit to the $\sigma(\mathrm{r})$ values inside of r_{a0}. Masses are shown beside the cluster name and the other cluster parameters are given in Table 2. The transition from stable to unstable orbits is shaded in grey and the indicative radius r_{chaos} is shown as the solid vertical lines. The vertical dashed red line shows where the acceleration is equal to the MOND value. The red dotted curve indicates the theoretical velocity dispersion for the quoted cluster mass.

analysis involving tidal effects on globular clusters, in particular on the velocity dispersion.

We find that an error in the cluster-galaxy orbital parameters, known to be very uncertain, is more likely than requiring new physics to explain the velocity dispersion in some clusters.

REFERENCES

Allen A. J., Richstone D. O., 1988, ApJ, 325, 583

Allen C., Moreno E., Pichardo B., 2006, ApJ, 652, 1150

Baumgardt H., Côté P., Hilker M., Rejkuba M., Mieske S., Djorgovski S. G., Stetson P., 2009, MNRAS, 396, 2051

Baumgardt H., Grebel E. K., Kroupa P., 2005, MRNAS, 359, L1

[!hp]

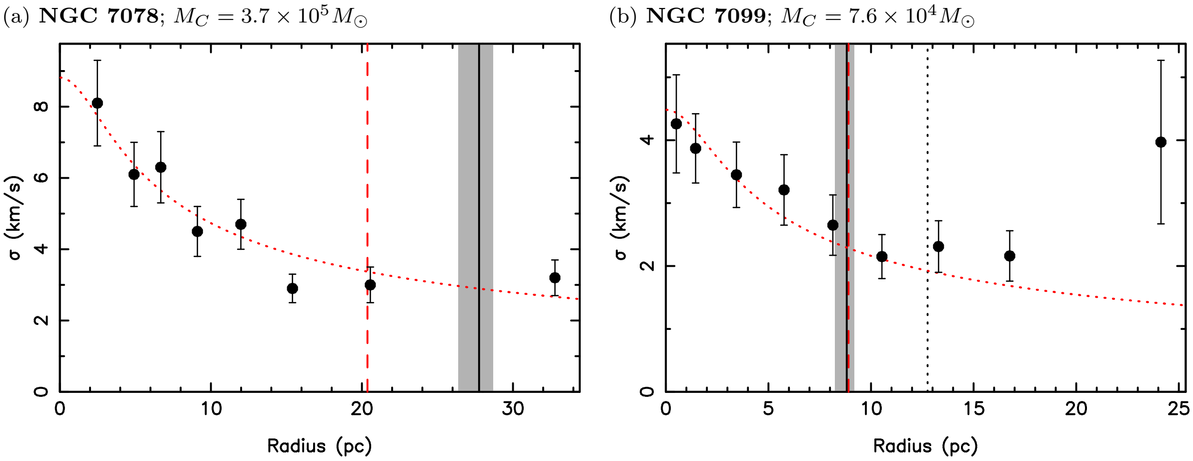

(a) **NGC 7078**; $M_C = 3.7 \times 10^5 M_\odot$

(b) **NGC 7099**; $M_C = 7.6 \times 10^4 M_\odot$

Figure 6. Figure 5 continued; fitted cluster masses used.

Baumgardt H., Mieske S., 2008, MNRAS, 391, 942

Bellazzini M., 2004, MNRAS, 347, 119

Binney J., Tremaine S., 1987, Galactic dynamics. Princeton, NJ, Princeton University Press, 1987

Dejonghe H., 1987, MNRAS, 224, 13

Di Criscienzo M., D'Antona F., Milone A. P., Ventura P., Caloi V., Carini R., D'Ercole Vesperini E., Piotto G., 2011, ArXiv e-prints

Dinescu D. I., Girard T. M., van Altena W. F., 1999, ApJ, 117, 1792

Dinescu D. I., Girard T. M., van Altena W. F., Mendez R. A., Lopez C. E., 1997, AJ, 114, 1014

Dinescu D. I., Majewski S. R., Girard T. M., Cudworth K. M., 2001, AJ, 122, 1916

Drukier G. A., Cohn H. N., Lugger P. M., Slavin S. D., Berrington R. C., Murphy B. W., 2007, AJ, 133, 1041

Drukier G. A., Slavin S. D., Cohn H. N., Lugger P. M., Berrington R. C., Murphy B. W., Seitzer P. O., 1998, AJ, 115, 708

Fellhauer M., Evans N. W., Belokurov V., Wilkinson M. I., Gilmore G., 2007, MNRAS, 380, 749

Fukushige T., Heggie D. C., 2000, MNRAS, 318, 753

Gentile G., Famaey B., Angus G., Kroupa P., 2010, A&A, 509, A97

Giersz M., Heggie D. C., 1994, MNRAS, 268, 257

Haghi H., Baumgardt H., Kroupa P., 2011, A&A, 527, A33

Harris W. E., 1996, AJ, 112, 1487

Ibata R., Sollima A., Nipoti C., Bellazzini M., Chapman S. C., Dalessandro E., 2011, ArXiv e-prints

Keenan D. W., 1981, A&A, 95, 340

Kennedy G., 2008, Ph.d. thesis, Monash University

Kennedy G. F., , 2011, this volume

King I., 1962, AJ, 67, 471

Lane R. R., Kiss L. L., Lewis G. F., Ibata R. A., Siebert A., Bedding T. R., Székely P., Balog Z., Szabó G. M., 2010, MNRAS, 406, 2732

Mardling R. A., , 2008a, in preparation

Mardling R. A., 2008b, in Aarseth S. J., Tout C. A., Mardling R. A., eds, Lecture Notes in Physics, Vol. 760: The Cambridge N-body Lectures Resonance, chaos and stability: the three-body problem in astrophysics

Meziane K., Colin J., 1996, A&A, 306, 747

Milgrom M., 1983, ApJ, 270, 365

Miyamoto M., Nagai R., 1975, PASJ, 27, 533

Moffat J. W., Toth V. T., 2008, ApJ, 680, 1158

Nipoti C., Ciotti L., Londrillo P., 2011, MNRAS, p. 608

Press W. B., Flannery B. P., Teukolsky S. A., Vettering W. T., 1986, Numerical Recipes: The Art of Scientific Computing. Cambridge Univ. Press, Cambridge

Scarpa R., Falomo R., 2010, A&A, 523, A43

Scarpa R., Marconi G., Carraro G., Falomo R., Villanova S., 2011, A&A, 525, A148

Scarpa R., Marconi G., Gilmozzi R., 2003, A&AL, 405, L15

Scarpa R., Marconi G., Gilmozzi R., 2004, in R. Dettmar, U. Klein, & P. Salucci ed., Baryons in Dark Matter Halos Using globular clusters to test gravity in the weak acceleration regime: NGC 6171

Scarpa R., Marconi G., Gilmozzi R., Carraro G., 2007a, The Messenger, 128, 41

Scarpa R., Marconi G., Gilmozzi R., Carraro G., 2007b, A&A, 462, L9

Sollima A., Nipoti C., 2010, MNRAS, 401, 131

Székely P., Kiss L. L., Szatmáry K., Csák B., Bakos G. Á., Bedding T. R., 2007, Astronomische Nachrichten, 328, 879